Elucidating the Facet-Dependent Selectivity for CO$_2$ Electroreduction to Ethanol of Cu−Ag Tandem Catalysts

Pranit Iyengar, Manuel J. Kolb, James R. Pankhurst, Federico Calle-Vallejo, and Raffaella Buonsanti*

Cite This: *ACS Catal.* 2021, 11, 4456−4463

Read Online

ACCESS | Metrics & More | Article Recommendations | Supporting Information

ABSTRACT: Despite being desirable high-value products of the electrochemical CO$_2$ reduction reaction (CO$_2$RR), alcohols are still obtained with lower selectivity compared to hydrocarbons and the reaction pathways leading to their formation are still under debate. In this joint experimental−computational work, we exploit structural sensitivity effects to elucidate the ethanol-producing active sites on Cu−Ag CO$_2$RR tandem catalysts. Specifically, methane-selective Cu nano-octahedra (Cu$_{oh}$), enclosed by (111) facets, and ethylene-selective Cu nanocubes (Cu$_{cub}$), enclosed by (100) facets, are mixed with CO-selective Ag nanospheres (Ag$_{sph}$) to form Cu$_{oh}$−Ag and Cu$_{cub}$−Ag bimetallic catalysts. Ethanol is selectively enhanced via the *CH$_x$−*CO coupling pathway at the terraces of Cu$_{oh}$−Ag in the CO-enriched environment generated by the Ag$_{sph}$. Conversely, on Cu$_{cub}$−Ag, ethanol is selectively produced via the same pathway at the edges and corners of Cu$_{cub}$, while ethylene continues to be produced at the terraces. The terraces being the predominant surfaces on the catalysts, such facet dependence explains the higher ethanol-to-ethylene ratio on the Cu$_{oh}$−Ag. These findings illustrate how tandem catalysis and structure-sensitive effects can be combined to obtain notable changes in the selectivity of electrochemical reactions.

KEYWORDS: facet-dependent selectivity, CO$_2$ electroreduction, ethanol, Cu−Ag tandem catalysts
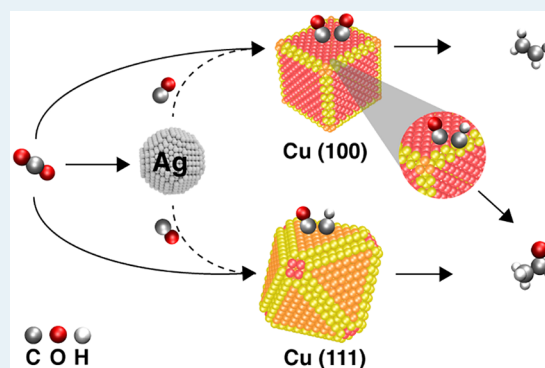
INTRODUCTION

The electrochemical CO$_2$ reduction reaction (CO$_2$RR) is a promising approach to mitigate the rising atmospheric CO$_2$ levels by converting it into fuels and chemical feedstocks, which becomes a means to store renewable energy.[1,2] Among single-metal surfaces, copper is the only catalyst capable of generating significant amounts of higher-value hydrocarbons and oxygenates.[1,3,4] Until now, most studies have focused on hydrocarbons and these efforts have resulted in Faradaic efficiencies (FEs) up to 83% for ethylene production.[5,6] Instead, while being extremely valuable products, alcohols are still obtained with considerably lower efficiencies.[1,2]

Recently, tandem schemes have emerged as a promising strategy to promote C$_{2+}$ and alcohols.[7−13] In these schemes, a CO-producing domain (i.e., Au, Ag, Zn, and Fe porphyrins) is coupled to a Cu catalyst. In all studies, the local enrichment of the CO intermediate is shown to suppress the competing hydrogen evolution reaction (HER) while enhancing the selectivity toward C$_{2+}$ products. In particular, ethanol (C$_2$H$_5$OH) and ethylene (C$_2$H$_4$) were both promoted in most cases.[7−9,11−13] The current state-of-the-art FE for C$_2$H$_5$OH is 41% and was achieved by functionalizing the Cu surface with CO-producing Fe porphyrin complexes, thus demonstrating the huge potential of tandem electrocatalysts.[11]

In general, the knowledge of the reaction pathways, strategies, and structural and compositional sensitivities favoring the formation of C$_2$H$_5$OH over C$_2$H$_4$ still remains limited.[11−19] A few experimental and computational studies have suggested that the pathways toward C$_2$H$_5$OH and C$_2$H$_4$ on Cu share several intermediates.[15,20] Li et al. calculated that, under high *CO coverage, the C$_2$H$_5$OH pathway is favored to a larger extent on Cu(111) with respect to Cu(100) via a mechanism that bifurcates from the C$_2$H$_4$ pathway several steps after *CO dimerization.[11] On the contrary, Ting et al. predicted that Cu(111) under high *CO coverage could stabilize the C$_2$H$_5$OH-yielding intermediate through a *CH$_x$−*CO coupling step, bypassing *CO dimerization.[12] Investigating the effect of elevated *CO coverages in the presence of Cu surfaces that favor either *CH$_x$ or dimerized *CO could aid in addressing this confusion, possibly leading to strategies to promote C$_2$H$_5$OH over C$_2$H$_4$. No experimental
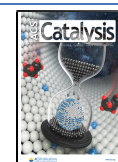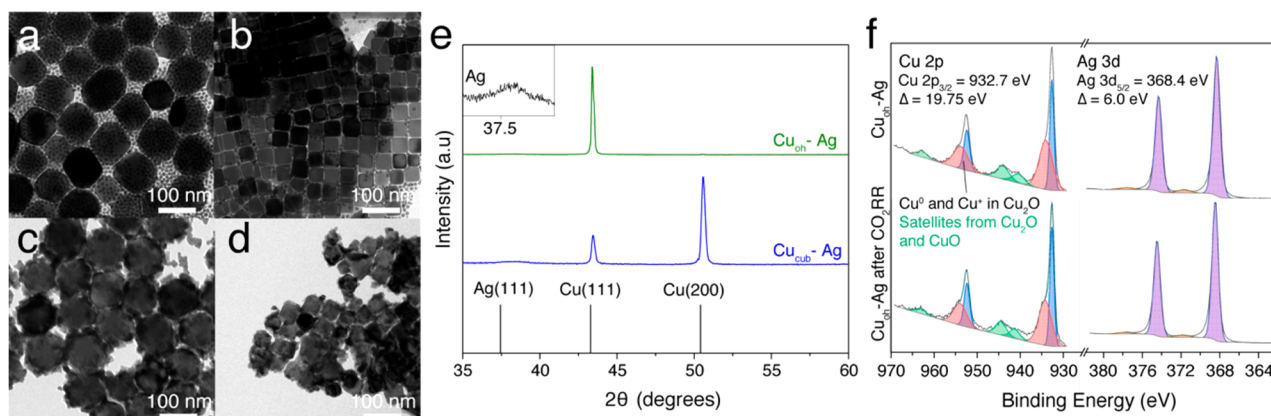
Figure 1. TEM images of (a) Cu_{oh}−Ag and (b) Cu_{cub}−Ag as prepared. TEM images of (c) Cu_{oh}−Ag and (d) Cu_{cub}−Ag after 15 min of electrolysis in 0.1 M $KHCO_3$ at −1.3 V_{RHE}. (e) XRD of the catalysts drop-cast onto a Si wafer (the inset shows a magnified Ag peak). (f) XPS analysis of the Cu_{oh}−Ag showing the Cu 2p and Ag 3d regions before and after 15 min of electrolysis in 0.1 M $KHCO_3$ at −1.3 V_{RHE}.

work has specifically investigated facet-dependent selectivity of tandem catalysis in CO_2RR so far.

Shape-controlled nanocrystals (NCs) have been demonstrated to be an ideal platform to translate into more realistic conditions the structure-dependent selectivity identified on metal single crystals.[6,21−28] In CO_2RR, Cu nano-octahedra (Cu_{oh}), enclosed by (111) facets, and Cu nanocubes (Cu_{cub}), enclosed by (100) facets, were found to be selective toward methane (CH_4) and ethylene (C_2H_4), respectively, in agreement with studies on Cu surfaces.[18,24,25,29−32] The facet-dependent selectivity of Cu NCs involves stabilization and high coverage of *CH_x species for CH_4 on Cu(111) and *CO−*CO coupling for C_2H_4 on Cu(100).[15,19,33,34]

Herein, we couple shape-controlled Cu NCs and Ag NCs to exploit structural effects in CO_2RR tandem catalysis and to elucidate the C_2H_5OH vs C_2H_4 branching point in the reaction pathway. Specifically, Cu_{oh} and Cu_{cub} are mixed with Ag nanospheres (Ag_{sph}) to form Cu_{oh}−Ag and Cu_{cub}−Ag bimetallic catalysts, respectively. In agreement with previous studies, our tandem catalysts display increasing C_{2+} and alcohol selectivity. At the same time, we show that the C_2H_5OH/C_2H_4 selectivity ratios attained on the Cu_{oh}−Ag are higher than those on the Cu_{cub}−Ag (2.4 vs 1.5) and are, to the best of our knowledge, among the highest reported on electronically unaltered Cu. Mechanistically speaking, we find that the alternative pathway via CH_x−CO coupling to produce ethanol can also be opened on (100) facets and, by virtue of its structural sensitivity, the production of C_2 species is boosted. However, on the Cu(111) facet, only the ethanol pathway is specifically enhanced without competition with the ethylene formation.

■ RESULTS AND DISCUSSION

In order to explore structural effects in tandem catalysts for the CO_2RR, we prepared Cu−Ag catalysts by homogeneously mixing Ag_{sph} with Cu_{oh} and Cu_{cub}, with average sizes of 9, 80, and 40 nm, respectively (Figure S1). These sizes were chosen as they were found in previous studies to be optimal for the production of CO, CH_4, and C_2H_4, respectively.[24,25,35]

Transmission electron microscopy (TEM) was used to characterize the morphology and structure of the two catalysts before and after the CO_2RR. The as-prepared catalysts consist of homogeneously mixed and well dispersed Cu and Ag NCs with a Cu:Ag mass ratio of 2:3 (Figure 1a,b). After only 15 min

of electrolysis, the Cu_{cub} and Cu_{oh} preserve their morphologies, while the Ag_{sph} forms a network structure intimately surrounding the Cu NCs (Figure 1c,d), in agreement with previous studies.[24,25,35] These structures remain unchanged after 1 h of operation. The corresponding X-ray diffraction (XRD) patterns (Figure 1e) evidence the characteristic features of the Cu_{oh} and Cu_{cub}, with preferential orientation along the (111) and (100) directions, respectively. The peak corresponding to the Ag NCs is less intense and broader due to the much smaller size of the crystallites. X-ray photoelectron spectra (XPS) (Figure 1f and Figure S2) of the Cu−Ag catalysts revealed that the Cu component is largely in its metallic state. The Cu $2p_{3/2}$ peaks appeared at similar values of 932.68 and 932.64 eV for the Cu_{cub} and Cu_{oh}, respectively. Both Cu−Ag catalysts also presented similar Ag $3d_{5/2}$ spectra, with the Ag $3d_{5/2}$ peaks appearing at 368.36 and 368.18 eV for the Cu_{cub}−Ag and Cu_{oh}−Ag, respectively. Additional loss features in the Ag $3d_{5/2}$ spectra indicate that Ag is in a metallic state, and the Ag MNN Auger spectra are also reminiscent of metallic Ag. Following the CO_2RR, both Cu_{oh}−Ag and Cu_{cub}−Ag presented near-identical XPS spectra; the Cu $2p_{3/2}$ and Ag $3d_{5/2}$ peaks were unchanged, as were the Cu LMM and Ag MNN Auger spectra. These results allow us to rule out major changes in electronic structure which would manifest via a more pronounced peak shifting.[36] While surface alloying limited to a few atomic layers cannot be completely excluded,[37,38] we expect any effect deriving from it to be the same in both Cu_{oh}−Ag and Cu_{cub}−Ag. Hence, any difference between the two systems can be interpreted within the framework of tandem catalysis, wherein an increasing local supply of CO is provided to the faceted Cu NCs.

The performance of the Cu_{oh}−Ag and Cu_{cub}−Ag catalysts for CO_2RR was evaluated in a typical H-type liquid cell with the catalysts drop-cast on flat glassy-carbon electrodes. Potentials were applied between −1.1 and −1.4 V_{RHE} (RHE: reversible hydrogen electrode); outside of this range, the Cu NCs alone yielded hydrogen as the major product, which is consistent with previous studies.[24,25,39,40]

Figure 2 reports the FEs toward gas and liquid products for Cu_{oh}−Ag (Figure 2a) and Cu_{cub}−Ag (Figure 2b), which are compared with the respective bare Cu NCs and Ag_{sph} at different potentials. All values at each potential are reported in Table S2. The following major trends are observed. With the exception of −1.1 V_{RHE}, the addition of Ag NCs suppresses the
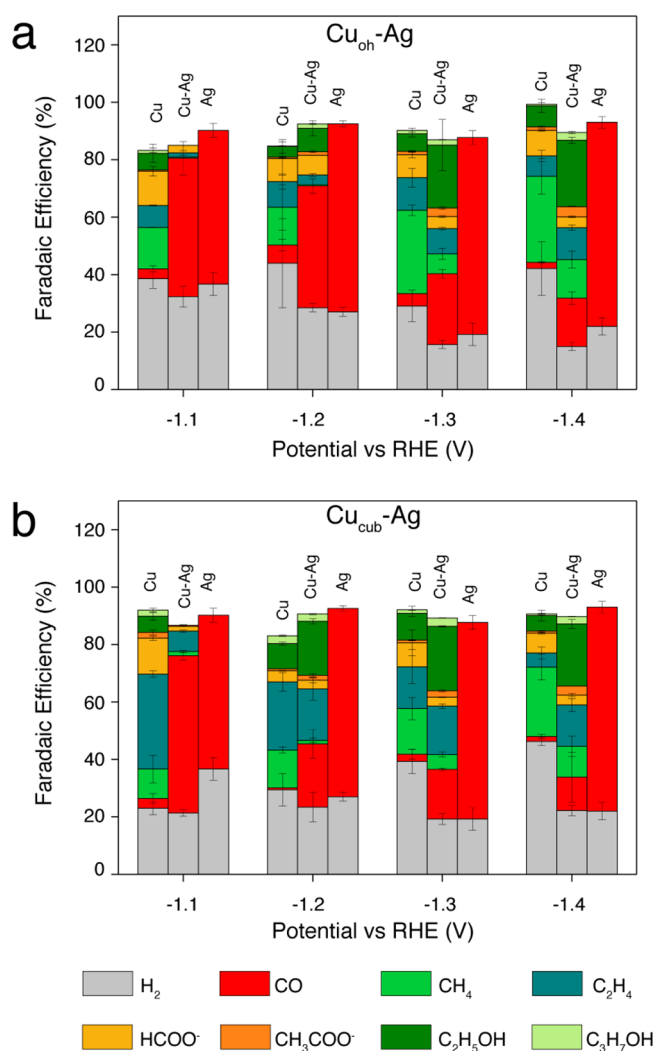
Figure 2. FEs for (a) Cu_{oh}−Ag and (b) Cu_{cub}−Ag at variable potentials, where the Cu mass loading is 15 $\mu g/cm^2$. For comparison, FEs are shown for the bare Cu and Ag NCs at the same loading. CO_2RR measurements were carried out using glassy-carbon electrodes as the substrate and CO_2-saturated 0.1 M $KHCO_3$ electrolyte. The reported values are averages of three independent experiments.

HER and enhances the CO_2RR on both the Cu_{oh} and Cu_{cub}. This result is in agreement with previous literature on tandem

catalysts and can be attributed to the local generation of CO.[9,41] At potentials more cathodic than −1.1 V_{RHE}, the CO FEs are dramatically lower on the Cu−Ag catalysts when compared to the bare Ag NCs, which is consistent with the CO formed on the Ag_{sph} being consumed by Cu via tandem catalysis. Values of the partial current densities and of the fractional CO_2 consumption support such a statement (Figure S3 and relative discussion in the Supporting Information). The CO FE decreases from 48.2 to 16.8% on Cu_{oh}−Ag and from 54.8 to 11.7% on Cu_{cub}−Ag as the potential shifts from −1.1 to −1.4 V_{RHE}, implying that the effectiveness of the tandem catalysis mechanism improves concomitantly with Cu becoming more efficient in converting CO.[8]

Turning toward a more detailed analysis of the CO_2RR products, the FE of CH_4 is suppressed on the Cu−Ag catalysts across the entire potential range. For example, it drops from 29% on the Cu_{oh} to 6.9% on the Cu_{oh}−Ag catalyst at −1.3 V_{RHE}. Similarly, it goes from 15.9% on the Cu_{cub} to 5.2% on the Cu_{cub}−Ag catalyst at −1.3 V_{RHE}. More cathodic potential promotes CO hydrogenation over C−C coupling, thereby promoting C_1 pathways enhancing CH_4 FE.[17,33]

Concerning the C_2 products, the FEs of C_2H_4 on the Cu_{oh} are in the 7−11.4% range from −1.1 V_{RHE} to −1.4 V_{RHE} and do not change appreciably in the Cu_{oh}−Ag catalyst. For Cu_{cub}, the C_2H_4 FE decreases steadily from 33.1% at −1.1 V_{RHE} to 4.9% at −1.4 V_{RHE}. Compared to these values, the FE of C_2H_4 for Cu_{cub}−Ag remains within the standard deviation of the measurements at −1.2 V_{RHE} (from 23.7 to 18%) and at −1.3 V_{RHE} (14.6 to 16.8%); instead, it increases at −1.4 V_{RHE} (4.9 to 14.4%). This shows that C_2H_4 active sites, namely, the dominant CO_2RR active sites on Cu_{cub}, possibly benefit from the local CO supply in the Cu_{cub}−Ag at a high overpotential.

The C_2H_5OH selectivity increases on both Cu−Ag catalysts compared to the bare Cu NCs. In particular, the C_2H_5OH FE increases from 3.7 to 8.1% at −1.2 V_{RHE}, 6.1 to 21.9% at −1.3 V_{RHE}, and 7.4 to 23.1% at −1.4 V_{RHE}, respectively, when comparing the Cu_{oh} with the Cu_{oh}−Ag. Similarly, on Cu_{cub}−Ag, the C_2H_5OH FE goes from 8.8 to 18.8%, 9.3 to 22.5%, and 5.4 to 21.6% at the same potentials when compared to the Cu_{cub}. Apart from the suppression of formate on the Cu−Ag catalysts with respect to the Cu NCs, no other major changes were observed in the liquid products. This finding is in agreement with the fact that no Cu−Ag alloying occurs in our catalysts, as the concurring electronic effect could have resulted in the generation of carbonyl-containing compounds.[37,42] We
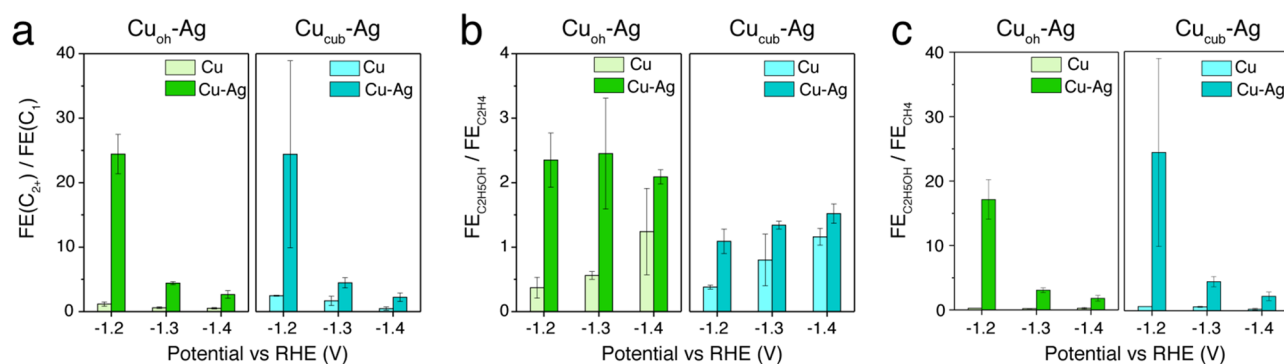

Figure 3. (a) $FE_{C_{2+}}/FE_{C_1}$, (b) $FE_{C_2H_5OH}/FE_{C_2H_4}$, and (c) $FE_{C_2H_5OH}/FE_{CH_4}$ for Cu_{oh}−Ag and Cu_{cub}−Ag at variable potentials, where the Cu mass loading is 15 $\mu g/cm^2$. The CO_2RR measurements were carried out using glassy-carbon electrodes as the substrate and CO_2-saturated 0.1 M $KHCO_3$ electrolyte. The reported values are averages of three independent experiments.
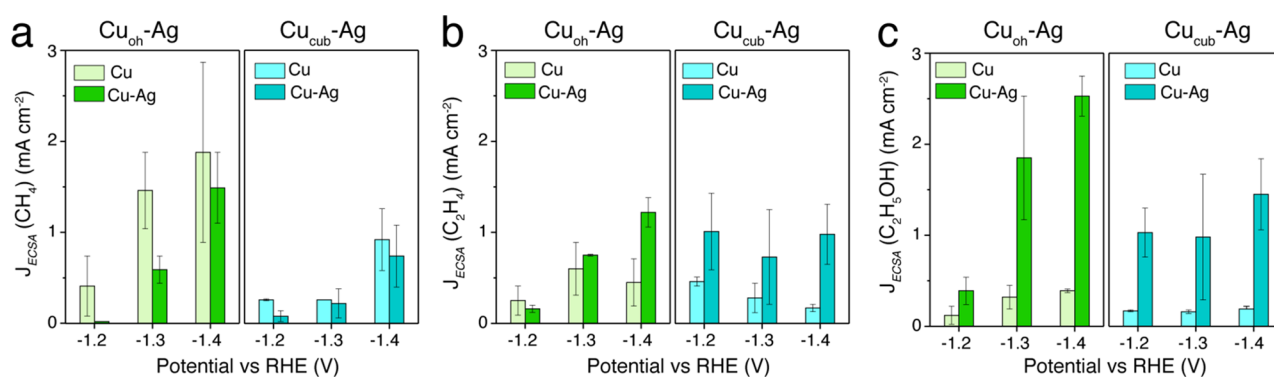
Figure 4. ECSA-normalized partial current densities (J_{ECSA}) for (a) CH_4, (b) C_2H_4, and (c) C_2H_5OH of the Cu_{oh}−Ag and Cu_{cub}−Ag catalysts, where the Cu mass loading is 15 $\mu g/cm^2$. CO_2RR measurements were carried out using glassy-carbon electrodes as the substrate and CO_2-saturated 0.1 M $KHCO_3$ electrolyte. The reported values are averages of three independent experiments. The total current densities are shown in Figure S5.

note that the Cu:Ag 2:3 mass ratio was found to be optimal with regard to consumption of the local amount of supplied CO (Figure S4).

To facilitate the comparison among samples and the identification of specific trends, Figure 3 shows the FE ratios of C_{2+}/C_1, C_2H_5OH/C_2H_4, and C_2H_5OH/CH_4 for Cu_{oh}−Ag and Cu_{cub}−Ag compared with the bare Cu NCs in the potential window where tandem catalysis was the most effective (-1.2 to -1.4 V_{RHE}). As observed in previous studies on tandem schemes,[7−13] the C_{2+}/C_1 ratios are higher on the Cu−Ag catalysts and they decrease on both the Cu and the Cu−Ag catalysts as the potential becomes more cathodic (Figure 3a), which is in agreement with more negative potentials favoring C_1 pathways over C−C coupling.[17,33] In terms of selectivity toward alcohols, Figure 3b illustrates an increased C_2H_5OH/C_2H_4 ratio on the Cu−Ag catalysts, which is more pronounced on the Cu_{oh}−Ag and at lower over-potentials.

A maximum ratio of 2.4 is observed on the Cu_{oh}−Ag at -1.3 V_{RHE}. Instead, the C_2H_5OH/C_2H_4 ratio on Cu_{cub}−Ag reaches a maximum of 1.5 at -1.4 V_{RHE}. Notably, the C_2H_5OH/CH_4 ratio increases 2 orders of magnitude on both bimetallic catalysts as compared to the respective bare Cu NCs at the lowest potential (Figure 3c). Indeed, it goes from below 1.0 on the Cu_{oh} and Cu_{cub} to 17.1 and 24.4 on Cu_{oh}−Ag and Cu_{cub}−Ag, respectively.

To assess whether these trends are related to an increased rate of ethanol production or to a suppression of the methane pathway, the partial current densities for methane, ethylene, and ethanol are plotted in Figure 4 for the two Cu−Ag catalysts.

Figure 4 reports the partial current densities normalized by the electrochemically active surface area (ECSA) for the catalysts studied. Notably, $J_{ECSA}(CH_4)$ decreases on both Cu_{oh}−Ag and Cu_{cub}−Ag compared to the bare Cu NCs at all potentials (Figure 4a), indicating that the production rate of methane is actually suppressed. Instead, $J_{ECSA}(C_2H_4)$ and $J_{ECSA}(C_2H_5OH)$ clearly increase on both catalysts (Figure 4b and c). However, while the absolute values of $J_{ECSA}(C_2H_4)$ on both bimetallic catalysts are quite similar to each other, $J_{ECSA}(C_2H_5OH)$ is considerably higher on the Cu_{oh}−Ag catalysts than on Cu_{cub}−Ag. For example, $J_{ECSA}(C_2H_5OH)$ reaches 2.5 mA/cm^2 on Cu_{oh}−Ag and 1.4 mA/cm^2 on Cu_{cub}−Ag at -1.4 V_{RHE}. Concomitantly, the enhancement factors for CH_4, C_2H_4, and C_2H_5OH clearly show that, on the Cu_{cub}−Ag, the production of both ethylene and ethanol is enhanced;

instead, on the Cu_{oh}−Ag, the ethanol pathway is selectively promoted (Figure S6).

As mentioned in the Introduction, a consensus on the ethanol formation pathway is yet to be reached. Most of the reports support the hypothesis that the C_2H_5OH vs C_2H_4 bifurcation occurs after CO dimerization.[11,15,19,33] Only a few studies have proposed the bifurcation to happen prior to CO dimerization (via *CH_x−*CO coupling).[12,13] As a reminder, the Cu_{oh} are enclosed by (111) facets, which are intrinsically more selective toward methane.[24] CH_4 active sites probably have an appreciable coverage of *CH, *CH_2, and/or *CH_3 intermediates. When supplied with a high local concentration of CO, these intermediates may couple with it before undergoing further reduction.[1] Indeed, Ting et al. suggested *CH or *CH_2 coupling with *CO and further reducing to C_2H_5OH in an ethanol-selective pathway that is favorable on Cu(111) only under elevated *CO coverage.[12] Such a prediction is consistent with our results. At this point, we decided to look further into the structural sensitivity of ethanol evolution via *CH_x−*CO coupling by computationally studying it on stepped Cu(100) surfaces, bearing in mind that previous studies did so for Cu(111) terraces and that step sites at Cu(111) likely remain methane-selective at high CO coverage.[12]

First of all, the highly favorable production of CO from CO_2 on Ag nanoparticles and extended surfaces is well-known.[12,43,44] Therefore, in the following, we will focus on the coupling between *CH_x and *CO and the subsequent reduction of *CHCO to C_2H_5OH. We calculated the kinetic barriers for *CH and *CH_2 coupling with CO, since these will strongly determine if the alternative pathway that circumvents *CO dimerization is open or not. The calculations were performed for both the terrace and the step of a Cu(711) surface. The (711) terraces correspond to the (100) facets of the cubes; instead, the (711) steps correspond to the edges of the cubes (Figure S7). The barriers shown in Table 1 for *CO coupling with *CH differ drastically for the step and terrace sites of Cu(711), with little to no coupling barrier (0.09 eV) for the step edge and a large one on the terrace (1.32 eV). We also calculated the kinetic barrier for the association of *CO and *CH_2 and found a substantial yet surmountable coupling barrier (0.49 eV) for the step edge and a larger one at the terrace (0.85 eV). In both cases, the barriers are lower at the steps compared to the terraces. In brief, we conclude that the edges should be highly active for *CH + *CO coupling and

Table 1. Calculated Barriers (in eV) for *CO Association with *CH and *CH$_2$ on the Cu(711) Step-Edge and Terrace Sites[a]

coupling step	barrier on the (100) terrace of Cu(711)	barrier on the step edge of Cu(711)	barrier on Cu(111)
*CO + *CH	1.32	0.09	0.70
*CO + *CH$_2$	0.85	0.49	0.71

[a]For comparison, data for the flat Cu(111) surface are provided, taken from the work by Ting et al.[12]

modestly active for *CH$_2$ + *CO coupling. Conversely, the analogous coupling reactions at terraces are unlikely.

Moving forward along the reaction pathway toward ethanol, we calculated the minimum-energy pathway for the reaction intermediates starting from *CHCO. The results obtained from these calculations are shown in Figure 5, while a more detailed view on other possible intermediates, including the *CH$_2$CO intermediate, for both the step and terrace sites is shown in Figure S8. Our results indicate that the most stable intermediates along the reaction pathway are identical to those found on Cu(111).[12] However, the energetics are quantitatively different, as Cu(111) terraces bind the CO$_2$RR intermediates more weakly than Cu(100) terraces and steps, in line with previous observations for C$_1$ intermediates.[45,46]

We note that C$_2$ species are readily formed on Cu(100) sites via *CO–*CO coupling and that Cu(100) usually favors ethylene production over ethanol.[1–3] Thus, increasing the *CO coverage on the Cu(711) terraces should not enhance the production of ethanol with respect to ethylene. Along these lines, for Cu$_{cub}$–Ag, the enhancement in ethanol production probably stems only from edge and corner sites. In the following, we will analyze the implications of this conclusion (see full details in section 2.4 in the Supporting Information). The partial current densities (J_i) (for i = ethylene and ethanol) can be expressed as the sum of the current densities of the active sites, which comprise (100) terraces and defects such as edges and corners ($J_i = J_i^{terraces} + J_i^{defects}$) Since ethylene and ethanol both require 12 electrons to be obtained from CO$_2$RR,

the ratio of their partial current densities is equivalent to the ratio of Faradaic efficiencies. Given that ethylene is mostly produced on the (100) terraces, we have the following approximation for Cu$_{cub}$:

$$\left(\frac{FE_{C_2H_5OH}}{FE_{C_2H_4}}\right)_{Cu_{cub}} \approx \left(\frac{J_{C_2H_5OH}^{terraces} + J_{C_2H_5OH}^{defects}}{J_{C_2H_4}^{terraces}}\right) \tag{1}$$

The ratio of Faradaic efficiencies for the Cu$_{cub}$–Ag tandem catalyst is the same as that for Cu$_{cub}$, except for an additional term that accounts for the activity of step sites owed to the *CH–*CO pathway. This leads to eq 2, which connects the ratio of the Faradaic efficiencies in the bare Cu cubes and in the Cu–Ag catalyst

$$\left(\frac{FE_{C_2H_5OH}}{FE_{C_2H_4}}\right)_{Cu_{cub}-Ag}$$

$$\approx \left(\frac{FE_{C_2H_5OH}}{FE_{C_2H_4}}\right)_{Cu_{cub}} + \frac{A_{C_2H_5OH}^{defects}}{A_{C_2H_4}^{terraces}} e^{-0.5(\Delta G_{C_2H_5OH}^{\#} - \Delta G_{C_2H_4}^{\#})/k_BT} \tag{2}$$

where 0.5 is a typical value for the symmetry factor,[47] $\Delta G_i^{\#}$ is the activation free energy of the rate-limiting step, and A_i are surface areas. From the experiments in Figure 3b, the average $(FE_{C_2H_5OH}/FE_{C_2H_4})_{Cu_{cub}-Ag} \approx 1$, whereas $(FE_{C_2H_5OH}/FE_{C_2H_4})_{Cu_{cub}} \approx 0.5$. Since the area occupied by edge and kink sites on a 40 nm Cu cube is approximately 2.6% of the area occupied by the terrace sites (where *CO–*CO dimerization is still favorable and leads to ethylene), we conclude that the exponential term in eq 2 is 19.2. Thus, on Cu$_{cub}$–Ag, the ethanol-producing edges and corners are roughly 19 times more active than ethylene-producing terrace sites, but they are not abundant. Conversely, considering the predominance of (111) terraces on the Cu$_{oh}$ and the relative unfavorability of competing *CO–*CO dimerization pathways, it is possible to rationalize why Cu$_{oh}$–Ag catalysts selectively promote ethanol.
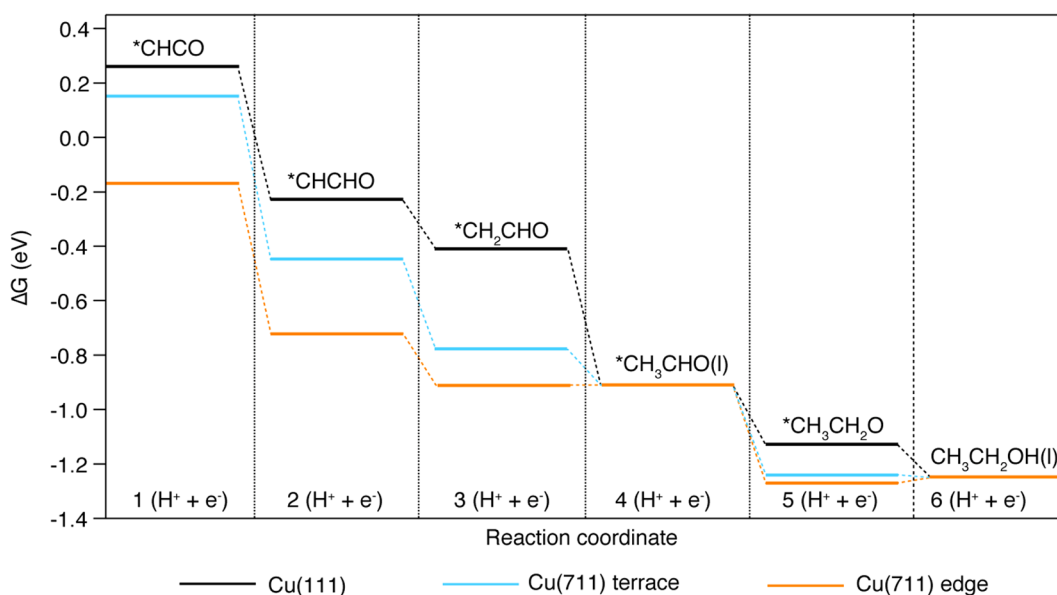

Figure 5. Reaction energies for the most stable intermediates along the *CHCO reduction pathway to ethanol at 0 V vs RHE. Data for Cu(111) were adapted from previous work.[12]

CONCLUSIONS

The facet-dependent CO_2RR selectivity of Cu catalysts in a tandem configuration was studied using Cu_{oh}, terminated by (111) facets, and Cu_{cub}, terminated by (100) facets, with CO-producing Ag_{sph}. Both Cu–Ag catalysts showed enhanced selectivity and activity for C_2H_5OH and C_2H_4 and suppressed selectivity and activity for CH_4 and H_2. At the same time, we found a considerably higher selectivity toward C_2H_5OH on the Cu_{oh}–Ag catalysts with the C_2H_5OH/C_2H_4 ratio reaching 2.4 versus 1.5 on the Cu_{cub}–Ag catalyst under the same conditions. To the best of our knowledge, this value represents the state of the art in the C_2H_5OH/C_2H_4 ratio from electronically unaltered Cu electrodes.

DFT calculations and a simple model evidenced that, under high *CO coverage, the active sites on Cu_{cub}–Ag catalyst responsible for the enhancement of ethanol production are located at edge and corner sites and favor $*CH_x$ and *CO coupling and its subsequent reduction, while the more extended (100) facets still promote ethylene. In addition, the (111) facets on Cu_{oh}–Ag catalyst also catalyze the $*CH_x$–*CO coupling and following reduction to C_2H_5OH. Since the ethanol-producing active sites are in greater number on Cu_{oh}–Ag compared to Cu_{cub}–Ag catalyst, it follows that the ethanol selectivity of Cu_{oh}–Ag catalysts is larger.

Overall, our results suggest that a catalyst exhibiting a high selectivity for CH_4 (thereby harboring a dense population of $*CH_x$ intermediates under reaction conditions) should yield high C_2H_5OH FEs under a local excess of CO. Additionally, the theoretical findings suggest that a boost to the ethanol selectivity of Cu_{cub}–Ag could be achieved by using particles with high defect-to-terrace ratios, which will be the aim of future studies.

ASSOCIATED CONTENT

Ⓢ Supporting Information

The Supporting Information is available free of charge at https://pubs.acs.org/doi/10.1021/acscatal.1c00420.

> Chemicals used, synthesis protocols, structural characterization, electrode preparation and CO_2RR analysis method, electrochemical data, solvent contributions to free energies, adsorption energies, kinetic barrier, and optimized geometries used in DFT calculations (PDF)

AUTHOR INFORMATION

Corresponding Author

Raffaella Buonsanti − *Laboratory of Nanochemistry for Energy (LNCE), Institute of Chemical Sciences and Engineering (ISIC), École Polytechnique Fédérale de Lausanne, CH-1950 Sion, Switzerland;* ⓘ orcid.org/0000-0002-6592-1869; Email: raffaella.buonsanti@epfl.ch

Authors

Pranit Iyengar − *Laboratory of Nanochemistry for Energy (LNCE), Institute of Chemical Sciences and Engineering (ISIC), École Polytechnique Fédérale de Lausanne, CH-1950 Sion, Switzerland*

Manuel J. Kolb − *Department of Materials Science and Chemical Physics & Institute of Theoretical and Computational Chemistry (IQTCUB), University of Barcelona, 08028 Barcelona, Spain;* ⓘ orcid.org/0000-0003-2878-6976

James R. Pankhurst − *Laboratory of Nanochemistry for Energy (LNCE), Institute of Chemical Sciences and Engineering (ISIC), École Polytechnique Fédérale de Lausanne, CH-1950 Sion, Switzerland*

Federico Calle-Vallejo − *Department of Materials Science and Chemical Physics & Institute of Theoretical and Computational Chemistry (IQTCUB), University of Barcelona, 08028 Barcelona, Spain*

Complete contact information is available at:
https://pubs.acs.org/10.1021/acscatal.1c00420

Notes

The authors declare no competing financial interest.

ACKNOWLEDGMENTS

REFERENCES

(1) Nitopi, S.; Bertheussen, E.; Scott, S. B.; Liu, X.; Engstfeld, A. K.; Horch, S.; Seger, B.; Stephens, I. E. L.; Chan, K.; Hahn, C.; Nørskov, J. K.; Jaramillo, T. F.; Chorkendorff, I. Progress and Perspectives of Electrochemical CO_2 Reduction on Copper in Aqueous Electrolyte. *Chem. Rev.* **2019**, *119*, 7610−7672.

(2) Birdja, Y. Y.; Pérez-Gallent, E.; Figueiredo, M. C.; Göttle, A. J.; Calle-Vallejo, F.; Koper, M. T. M. Advances and Challenges in Understanding the Electrocatalytic Conversion of Carbon Dioxide to Fuels. *Nat. Energy* **2019**, *4*, 732−745.

(3) Gattrell, M.; Gupta, N.; Co, A. A Review of the Aqueous Electrochemical Reduction of CO2 to Hydrocarbons at Copper. *J. Electroanal. Chem.* **2006**, *594*, 1−19.

(4) Kuhl, K. P.; Cave, E. R.; Abram, D. N.; Jaramillo, T. F. New Insights into the Electrochemical Reduction of Carbon Dioxide on Metallic Copper Surfaces. *Energy Environ. Sci.* **2012**, *5*, 7050−7059.

(5) Dinh, C.; Burdyny, T.; Kibria, G.; Seifitokaldani, A.; Christine, M. CO_2 Electroreduction to Ethylene via Hydroxide-Mediated Copper Catalysis at an Abrupt Interface. *Science* **2018**, *787*, 783−787.

(6) Zhang, B.; Zhang, J.; Hua, M.; Wan, Q.; Su, Z.; Tan, X.; Liu, L.; Zhang, F.; Chen, G.; Tan, D.; Cheng, X.; Han, B.; Zheng, L.; Mo, G. Highly Electrocatalytic Ethylene Production from CO_2 on Nanodefective Cu Nanosheets. *J. Am. Chem. Soc.* **2020**, *142*, 13606−13613.

(7) Li, Y. C.; Wang, Z.; Yuan, T.; Nam, D.-H.; Luo, M.; Wicks, J.; Chen, B.; Li, J.; Li, F.; de Arquer, F. P. G.; Wang, Y.; Dinh, C.-T.; Voznyy, O.; Sinton, D.; Sargent, E. H. Binding Site Diversity Promotes CO_2 Electroreduction to Ethanol. *J. Am. Chem. Soc.* **2019**, *141*, 8584−8591.

(8) Morales-Guio, C. G.; Cave, E. R.; Nitopi, S. A.; Feaster, J. T.; Wang, L.; Kuhl, K. P.; Jackson, A.; Johnson, N. C.; Abram, D. N.; Hatsukade, T.; Hahn, C.; Jaramillo, T. F. Improved CO2 Reduction Activity towards C2+ Alcohols on a Tandem Gold on Copper Electrocatalyst. *Nat. Catal.* **2018**, *1*, 764−771.

(9) Lum, Y.; Ager, J. W. Sequential Catalysis Controls Selectivity in Electrochemical CO2 Reduction on Cu. *Energy Environ. Sci.* **2018**, *11*, 2935−2944.

(10) Chen, C.; Li, Y.; Yu, S.; Louisia, S.; Jin, J.; Li, M.; Ross, M. B.; Yang, P. Cu−Ag Tandem Catalysts for High-Rate CO2 Electrolysis toward Multicarbons. *Joule* **2020**, *4*, 1688−1699.

(11) Li, F.; Li, Y. C.; Wang, Z.; Li, J.; Nam, D.-H.; Lum, Y.; Luo, M.; Wang, X.; Ozden, A.; Hung, S.-F.; Chen, B.; Wang, Y.; Wicks, J.; Xu, Y.; Li, Y.; Gabardo, C. M.; Dinh, C.-T.; Wang, Y.; Zhuang, T.-T.; Sinton, D.; Sargent, E. H. Cooperative CO2-to-Ethanol Conversion via Enriched Intermediates at Molecule−Metal Catalyst Interfaces. *Nat. Catal.* **2020**, *3*, 75−82.

(12) Ting, L. R. L.; Piqué, O.; Lim, S. Y.; Tanhaei, M.; Calle-Vallejo, F.; Yeo, B. S. Enhancing CO2 Electroreduction to Ethanol on Copper-Silver Composites by Opening an Alternative Catalytic Pathway. *ACS Catal.* **2020**, *10*, 4059−4069.

(13) Ren, D.; Gao, J.; Pan, L.; Wang, Z.; Luo, J.; Zakeeruddin, S. M.; Hagfeldt, A.; Grätzel, M. Atomic Layer Deposition of ZnO on CuO Enables Selective and Efficient Electroreduction of Carbon Dioxide to Liquid Fuels. *Angew. Chem.* **2019**, *131*, 15178−15182.

(14) Schouten, K. J. P.; Kwon, Y.; van der Ham, C. J. M.; Qin, Z.; Koper, M. T. M. A New Mechanism for the Selectivity to C1 and C2 Species in the Electrochemical Reduction of Carbon Dioxide on Copper Electrodes. *Chem. Sci.* **2011**, *2*, 1902−1909.

(15) Calle-Vallejo, F.; Koper, M. T. M. Theoretical Considerations on the Electroreduction of CO to C_2 Species on Cu(100) Electrodes. *Angew. Chem., Int. Ed.* **2013**, *52*, 7282−7285.

(16) Bertheussen, E.; Verdaguer-Casadevall, A.; Ravasio, D.; Montoya, J. H.; Trimarco, D. B.; Roy, C.; Meier, S.; Wendland, J.; Nørskov, J. K.; Stephens, I. E. L.; Chorkendorff, I. Acetaldehyde as an Intermediate in the Electroreduction of Carbon Monoxide to Ethanol on Oxide-Derived Copper. *Angew. Chem., Int. Ed.* **2016**, *55*, 1450−1454.

(17) Ledezma-Yanez, I.; Gallent, E. P.; Koper, M. T. M.; Calle-Vallejo, F. Structure-Sensitive Electroreduction of Acetaldehyde to Ethanol on Copper and Its Mechanistic Implications for CO and CO2 Reduction. *Catal. Today* **2016**, *262*, 90−94.

(18) Hori, Y.; Takahashi, R.; Yoshinami, Y.; Murata, A. Electrochemical Reduction of CO at a Copper Electrode. *J. Phys. Chem. B* **1997**, *101*, 7075−7081.

(19) Luo, W.; Nie, X.; Janik, M. J.; Asthagiri, A. Facet Dependence of CO_2 Reduction Paths on Cu Electrodes. *ACS Catal.* **2016**, *6*, 219−229.

(20) Murata, A.; Hori, Y. Product Selectivity Affected by Cationic Species in Electrochemical Reduction of CO_2 and CO at a Cu Electrode. *Bull. Chem. Soc. Jpn.* **1991**, *64*, 123−127.

(21) Grosse, P.; Gao, D.; Scholten, F.; Sinev, I.; Mistry, H.; Roldan Cuenya, B. Dynamic Changes in the Structure, Chemical State and Catalytic Selectivity of Cu Nanocubes during CO_2 Electroreduction: Size and Support Effects. *Angew. Chem.* **2018**, *130*, 6300−6305.

(22) Li, Y.; Cui, F.; Ross, M. B.; Kim, D.; Sun, Y.; Yang, P. Structure-Sensitive CO2 Electroreduction to Hydrocarbons on Ultrathin 5-Fold Twinned Copper Nanowires. *Nano Lett.* **2017**, *17*, 1312−1317.

(23) Suen, N.-T.; Kong, Z.-R.; Hsu, C.-S.; Chen, H.-C.; Tung, C.-W.; Lu, Y.-R.; Dong, C.-L.; Shen, C.-C.; Chung, J.-C.; Chen, H. M. Morphology Manipulation of Copper Nanocrystals and Product Selectivity in the Electrocatalytic Reduction of Carbon Dioxide. *ACS Catal.* **2019**, *9*, 5217−5222.

(24) Iyengar, P.; Huang, J.; De Gregorio, G. L.; Gadiyar, C.; Buonsanti, R. Size Dependent Selectivity of Cu Nano-Octahedra Catalysts for the Electrochemical Reduction of CO_2 to CH_4. *Chem. Commun.* **2019**, *55*, 8796−8799.

(25) Loiudice, A.; Lobaccaro, P.; Kamali, E. A.; Thao, T.; Huang, B. H.; Ager, J. W.; Buonsanti, R. Tailoring Copper Nanocrystals towards C_2 Products in Electrochemical CO_2 Reduction. *Angew. Chem., Int. Ed.* **2016**, *55*, 5789−5792.

(26) Huang, J.; Buonsanti, R. Colloidal Nanocrystals as Heterogeneous Catalysts for Electrochemical CO_2 Conversion. *Chem. Mater.* **2019**, *31*, 13−25.

(27) Roberts, F. S.; Kuhl, K. P.; Nilsson, A. High Selectivity for Ethylene from Carbon Dioxide Reduction over Copper Nanocube Electrocatalysts. *Angew. Chem., Int. Ed.* **2015**, *54*, 5179−5182.

(28) Guntern, Y. T.; Okatenko, V.; Pankhurst, J.; Varandili, S. B.; Iyengar, P.; Koolen, C.; Stoian, D.; Vavra, J.; Buonsanti, R. Colloidal Nanocrystals as Electrocatalysts with Tunable Activity and Selectivity. *ACS Catal.* **2021**, *11*, 1248−1295.

(29) Huang, Y.; Handoko, A. D.; Hirunsit, P.; Yeo, B. S. Electrochemical Reduction of CO_2 Using Copper Single-Crystal Surfaces: Effects of CO* Coverage on the Selective Formation of Ethylene. *ACS Catal.* **2017**, *7*, 1749−1756.

(30) Pérez-Gallent, E.; Marcandalli, G.; Figueiredo, M. C.; Calle-Vallejo, F.; Koper, M. T. M. Structure- and Potential-Dependent Cation Effects on CO Reduction at Copper Single-Crystal Electrodes. *J. Am. Chem. Soc.* **2017**, *139*, 16412−16419.

(31) Hahn, C.; Hatsukade, T.; Kim, Y.-G.; Vailionis, A.; Baricuatro, J. H.; Higgins, D. C.; Nitopi, S. A.; Soriaga, M. P.; Jaramillo, T. F. Engineering Cu Surfaces for the Electrocatalytic Conversion of CO_2: Controlling Selectivity toward Oxygenates and Hydrocarbons. *Proc. Natl. Acad. Sci. U. S. A.* **2017**, *114*, 5918−5923.

(32) Schouten, K. J. P.; Qin, Z.; Pérez Gallent, E.; Koper, M. T. M. Two Pathways for the Formation of Ethylene in CO Reduction on Single-Crystal Copper Electrodes. *J. Am. Chem. Soc.* **2012**, *134*, 9864−9867.

(33) Todorova, T. K.; Schreiber, M. W.; Fontecave, M. Mechanistic Understanding of CO_2 Reduction Reaction (CO2RR) Toward Multicarbon Products by Heterogeneous Copper-Based Catalysts. *ACS Catal.* **2020**, *10*, 1754−1768.

(34) Garza, A. J.; Bell, A. T.; Head-Gordon, M. Mechanism of CO_2 Reduction at Copper Surfaces: Pathways to C_2 Products. *ACS Catal.* **2018**, *8*, 1490−1499.

(35) Pankhurst, J. R.; Guntern, Y. T.; Mensi, M.; Buonsanti, R. Molecular Tunability of Surface-Functionalized Metal Nanocrystals for Selective Electrochemical CO_2 Reduction. *Chem. Sci.* **2019**, *10*, 10356−10365.

(36) Huang, J.; Mensi, M.; Oveisi, E.; Mantella, V.; Buonsanti, R. Structural Sensitivities in Bimetallic Catalysts for Electrochemical CO2 Reduction Revealed by Ag-Cu Nanodimers. *J. Am. Chem. Soc.* **2019**, *141*, 2490−2499.

(37) Clark, E. L.; Hahn, C.; Jaramillo, T. F.; Bell, A. T. Electrochemical CO_2 Reduction over Compressively Strained CuAg Surface Alloys with Enhanced Multi-Carbon Oxygenate Selectivity. *J. Am. Chem. Soc.* **2017**, *139*, 15848−15857.

(38) Herzog, A.; Bergmann, A.; Jeon, H. S.; Timoshenko, J.; Kühl, S.; Rettenmaier, C.; Lopez Luna, M.; Haase, F. T.; Roldan Cuenya, B. Operando Investigation of Ag-Decorated Cu 2 O Nanocube Catalysts with Enhanced CO_2 Electroreduction toward Liquid Products. *Angew. Chem., Int. Ed.* **2021**, *60*, 7426.

(39) Huang, J.; Hörmann, N.; Oveisi, E.; Loiudice, A.; De Gregorio, G. L.; Andreussi, O.; Marzari, N.; Buonsanti, R. Potential-Induced Nanoclustering of Metallic Catalysts during Electrochemical CO2 Reduction. *Nat. Commun.* **2018**, *9*, 3117.

(40) De Gregorio, G. L.; Burdyny, T.; Loiudice, A.; Iyengar, P.; Smith, W. A.; Buonsanti, R. Facet-Dependent Selectivity of Cu Catalysts in Electrochemical CO_2 Reduction at Commercially Viable Current Densities. *ACS Catal.* **2020**, *10*, 4854−4862.

(41) Schreier, M.; Yoon, Y.; Jackson, M. N.; Surendranath, Y. Competition between H and CO for Active Sites Governs Copper-Mediated Electrosynthesis of Hydrocarbon Fuels. *Angew. Chem., Int. Ed.* **2018**, *57*, 10221−10225.

(42) Wang, L.; Higgins, D. C.; Ji, Y.; Morales-Guio, C. G.; Chan, K.; Hahn, C.; Jaramillo, T. F. Selective Reduction of CO to Acetaldehyde with CuAg Electrocatalysts. *Proc. Natl. Acad. Sci. U. S. A.* **2020**, *117*, 12572−12575.

(43) Rosen, J.; Hutchings, G. S.; Lu, Q.; Rivera, S.; Zhou, Y.; Vlachos, D. G.; Jiao, F. Mechanistic Insights into the Electrochemical Reduction of CO_2 to CO on Nanostructured Ag Surfaces. *ACS Catal.* **2015**, *5*, 4293−4299.

(44) Clark, E. L.; Ringe, S.; Tang, M.; Walton, A.; Hahn, C.; Jaramillo, T. F.; Chan, K.; Bell, A. T. Influence of Atomic Surface Structure on the Activity of Ag for the Electrochemical Reduction of CO_2 to CO. *ACS Catal.* **2019**, *9*, 4006−4014.

(45) Calle-Vallejo, F.; Koper, M. T. M. Accounting for Bifurcating Pathways in the Screening for CO_2 Reduction Catalysts. *ACS Catal.* **2017**, *7*, 7346−7351.

(46) Durand, W. J.; Peterson, A. A.; Studt, F.; Abild-Pedersen, F.; Nørskov, J. K. Structure Effects on the Energetics of the Electrochemical Reduction of CO2 by Copper Surfaces. *Surf. Sci.* **2011**, *605*, 1354−1359.

(47) Guidelli, R.; Compton, R. G.; Feliu, J. M.; Gileadi, E.; Lipkowski, J.; Schmickler, W.; Trasatti, S. Defining the Transfer Coefficient in Electrochemistry: An Assessment (IUPAC Technical Report). *Pure Appl. Chem.* **2014**, *86*, 245−258.